Comparison of the electronic structure of anatase and rutile TiO_2 single-crystal surfaces using resonant photoemission and x-ray absorption spectroscopy

A. G. Thomas,* W. R. Flavell, A. K. Mallick, A. R. Kumarasinghe, D. Tsoutsou, N. Khan, C. Chatwin, S. Rayner, and G. C. Smith
School of Physics and Astronomy, University of Manchester, Sackville Street Building, P.O. Box 88, Manchester M60 1QD, United Kingdom

R. L. Stockbauer
Louisiana State University, Baton Rouge, Louisiana 70803, USA

S. Warren†
ESRF, Polygone Scientifique Louis Néel, 6, rue Jules Horowitz, 38000 Grenoble, France

T. K. Johal, S. Patel, and D. Holland
CCLRC, Daresbury Laboratory, Warrington, Cheshire WA5 4AD, United Kingdom

A. Taleb‡ and F. Wiame§
LURE, Universitaire Paris-Sud, Boîte Postale 34-91898 Orsay, France

(Received 17 July 2006; revised manuscript received 20 October 2006; published 5 January 2007)

A comparison of the electronic structure of rutile (110), anatase (101), and anatase (001) single-crystal surfaces has been made using resonant photoemission and x-ray absorption spectroscopy. Under identical preparative conditions, the anatase (101) surface shows the lowest Ti 3*d* and 4*sp* hybridization in the states close to the valence-band maximum of the three surfaces. It also shows the highest concentration of surface-oxygen vacancies. The effect on the electronic structure of modifying the surface preparative route and thus the concentration of surface-oxygen vacancies is examined. The σ-antibonding Ti 3*d* e_g/O 2*p* hybridization (probed by XAS) is reduced by the removal of surface-oxygen. Photoemission shows that as the number of surface-defects is increased, the O 2*p*-Ti 3*d* t_{2g} π-bonding interaction is disrupted. For the anatase (101) surface it is found that as the number of surface-oxygen vacancies is increased, the Ti 3*d* and 4*sp* contributions at the valence-band maximum are reduced. We discuss the correlation between electronic structure and photocatalytic activity of the different polymorphs of TiO_2.

DOI: 10.1103/PhysRevB.75.035105 PACS number(s): 73.20.At, 79.60.Bm

I. INTRODUCTION

TiO_2 has a number of technological uses including catalysis and photocatalysis.[1] Many of these applications utilize TiO_2 in its anatase phase rather than rutile, as this appears to be more catalytically active.[1] However, many of the fundamental studies of the reactivity of TiO_2 have concentrated on the rutile polymorph due to the ready availability of high-quality single crystals.[2–11] Recently, good-quality single crystals of anatase have become available which, coupled with advances in thin-film technology, have allowed detailed measurements of the electronic and topographic structure of the (101) and (001) surfaces.[12–14] However, to date, there has been no systematic comparison of the electronic structure of identically prepared rutile and anatase single-crystal surfaces, which in principle would allow connections to be made between electronic structure and surface reactivity. Such a comparison is one aim of the present work.

Both polymorphs are wide band-gap insulators when stoichiometric, with band gaps of 3.1 eV (rutile)[15] and 3.2 eV (anatase).[15] In both cases, the valence band is made up predominantly of O 2*p* states, with some Ti 3*d* and Ti 4*sp* character acquired through hybridization with the empty Ti 3*d*/4*sp* conduction-band states. Both polymorphs lose oxygen easily from the surface and bulk on heating to temperatures of around 500–700 °C. This results in an *n*-type semiconductor containing oxygen vacancies, which can be written as TiO_{2-x}.[5] The presence of O vacancies at the surface and the associated defect electrons, which remain localized as Ti^{3+} ions, results in the appearance of a defect peak or band-gap state at around 1 eV binding energy (BE), between the valence band and the Fermi energy.[2–5,12] Clearly, as the low-binding energy states may be accessed during a catalytic redox cycle, in the case of unreduced surfaces, the atomic character of the states close to the valence-band maximum (VBM) may be of importance in determining the catalytic activity of the surface. For reduced surfaces, the presence of defect states at around 1 eV from the Fermi energy is likely to have a substantial influence on the reactivity of the surface, through changes in both the electronic structure of the surface and in the geometric structure caused by the presence of oxygen defects.

Studies of the electronic structure of the anatase valence band have revealed that there is a difference in the population of Ti 3*d* and 4*sp* states at the VBM between the (101) and (001) anatase surfaces.[12] To the best of our knowledge, there has been no similar study of the Ti 3*d*/4*sp* contribution to the VBM of rutile TiO_2, although there have been previ-

ous studies of the atomic character of the main valence-band features.[2–4] In the case of the rutile (110) surface, different methods of preparation of the surface are found to give rise to different surface structures[5] and the concentration of oxygen vacancies is strongly dependent on the history of the sample.[5,16] For example, the stoichiometric surface produced by annealing a pale blue crystal in O_2 is different to that formed when a dark colored (heavily reduced) crystal is used.[5] Several studies have shown that water adsorption and dissociation is enhanced on surfaces containing O defects.[17] Thus it is clear that the reactivity of TiO_2 surfaces may be affected both by intrinsic differences in surface electronic structure between polymorphs and also by the surface oxygen defect concentration. In this work we explore the electronic structure of single-crystal surfaces as a function of both of these variables.

We have used resonant photoemission to probe the filled density-of-states function, while information about the empty states is obtained from x-ray absorption spectroscopy (XAS). Resonant photoemission spectroscopy is especially powerful in this context and has been used to probe the transition-metal contribution to the valence band in a number of systems.[2,3,6,18–20] It utilizes a measured increase or decrease in amplitude of certain photoemission spectral features as the photon energy is swept through the optical absorption edge of a constituent atom of the material. The direct Ti $3p$ photoemission process is given by

$$3p^6 3d^n + h\nu \rightarrow 3p^6 3d^{n-1} + e^-. \quad (1)$$

However, at the $3p \rightarrow 3d$ optical-absorption edge, a resonance due to interference between the direct photoemission process and the excitation of electrons from the $3p$ to the $3d$ orbital followed by a super-Coster-Kronig decay into a continuum state is observed,

$$3p^6 3d^n + h\nu \rightarrow [3p^5 3d^{n+1}]^* \rightarrow 3p^6 3d^{n-1} + e^-. \quad (2)$$

The asterisk denotes an excited state. Similarly, at the $3p \rightarrow 4s$ optical-absorption edge we have

$$3p^6 3d^m 4s^n + h\nu \rightarrow [3p^5 3d^m 4s^{n+1}]^* \rightarrow 3p^6 3d^m 4s^{n-1} + e^{-}. \quad (3)$$

The Ti $3d$ and $4sp$ levels in TiO_2 are of course unoccupied so one would not expect such resonances to occur. However, it is known that when there is strong hybridization between the O $2p$ and Ti $3d/4sp$ levels, then the resonance will occur via an interatomic process.[6] In this case then, the resonant excitation process (for $3d$ orbitals) occurs initially as in Eq. (2), but the decay channel is via the O $2p$ orbitals,[6] thus

$$[\mathrm{Ti}3p^5 3d^1]^* + \mathrm{O}2p^6 \rightarrow \mathrm{Ti}3p^6 3d^0 + \mathrm{O}2p^5 + e^-. \quad (4)$$

Similarly, hybridization between O $2p$ and Ti $4sp$ leads to resonance at the Ti $3p$-Ti $4s(p)$ resonance edge,[2,6]

$$\mathrm{Ti}\ 3p^6 3d^0 4s^0 + \mathrm{O}\ 2p^6 + h\nu \rightarrow [\mathrm{Ti}\ 3p^5 3d^0 4s^1]^* \mathrm{O}\ 2p^6 \rightarrow \mathrm{Ti}\ 3p^6 3d^0 4s^0 + \mathrm{O}\ 2p^5 + e^-. \quad (5)$$

Clearly, resonant excitations to $4p$ are dipole forbidden and thus are not observed unless there is some sp hybridization.

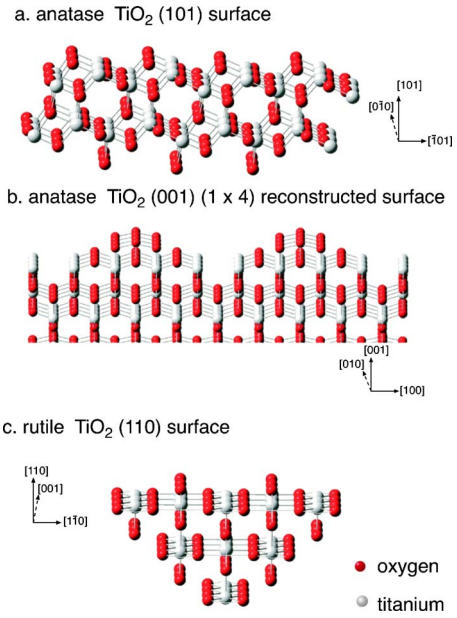

FIG. 1. (Color online) Side view ball and stick models of (a) the anatase (101) surface, (b) the anatase (001) (1×4) surface reconstruction, and (c) the rutile (110) surface. In the case of the (001) (1×4) reconstructed surface, a number of models of the reconstruction have been proposed (Refs. 14 and 21–23) We have chosen to illustrate the structure proposed by Liang *et al.*(Ref. 21).

In this paper we investigate the effects on the electronic structure of the anatase (001) and (101) and rutile (110) surfaces of a series of preparation methods. These surfaces are illustrated in Fig. 1. Resonant photoemission allows us to map the contributions to the TiO_2 valence band from the Ti $3d$ and $4sp$ states and thereby understand something of the changes in hybridization occurring following these different surface-preparation procedures. In addition, we present XAS spectra taken at the Ti L edge ($2p$) and O K edge (O $1s$) for the surfaces, which give information on the lowest unoccupied states. We compare the atomic character of the density-of-states function at the VBM for rutile and anatase surfaces and hence comment on the catalytic activity of these surfaces.

II. EXPERIMENTAL

Resonant photoemission experiments and XAS measurements were performed at the CCLRC Daresbury Laboratory SRS on beamlines 5D, 5U.1,[24,25] and MPW6.1 (Ref. 26) and on beamline SU3 of Super ACO at LURE.[27] Experiments on beamlines 5D and MPW6.1 utilized the ARUPS10 (Ref. 28) end station, which is fitted with a 100 mm mean radius rotatable multichannel detector analyzer, Ar^+ ion source, sample e-beam heating, LEED, and an electron gun for Auger electron spectroscopy. The sample was placed at around 45° to the incoming photons and electrons collected in normal emission mode. The XAS data were recorded in partial yield mode using a VSW hemispherical analyzer at 40° to the incoming photons. Photoemitted electrons were collected

in normal emission at kinetic energies (K.E.) of 374 eV (Ti 2*p* edge) and 506 eV (O 1*s* edge). The end station at LURE was the PES3 end station, again equipped with standard sample preparation instrumentation and a fixed SCIENTA 300 mm mean radius hemispherical analyzer.

The samples were single crystals of anatase with surfaces of (101) and (001) orientation, of size 2×5 mm and 2×3 mm, respectively (grown and supplied by Michael Grätzel and Roland Hengerer at the EPF Lausanne, Switzerland[29]) and a 10 mm$\times$10 mm rutile (110) single crystal (Pikem Ltd., UK). The anatase samples were black in color as observed by eye. The rutile single crystal was transparent initially but became pale blue/green following several sputter anneal cycles indicating bulk reduction of the sample.[5] All three samples were subjected to identical cycles of 1 keV Ar^+ ion sputtering for 10 min followed by 20 min annealing at 700 °C. These cycles were repeated until AES indicated them to be free of contaminants and sharp (1×1) LEED patterns were observed for the anatase (101) (Refs. 13 and 29) and rutile (110) crystals.[5,17] A (1×4) LEED pattern was obtained for the anatase (001) surface.[14,29] The samples were held on the sample manipulator by means of Ta clips. All energy-distribution-curve (EDC) spectra are referenced to a Fermi edge recorded from the Ta clips holding the samples in place and normalized to the incident photon flux. Constant initial-state (CIS) spectra were generated by taking the intensity of the background-subtracted EDCs at a fixed binding energy over a range of photon energies from 30 to 80 eV.

III. RESULTS AND DISCUSSION

A. Identically prepared, ordered surfaces

1. Valence band photoemission: General features

Figure 2 shows valence band EDCs recorded from anatase (101) (1×1), anatase (001) (1×4), and rutile (110) (1×1), surfaces, which were sputtered and annealed in UHV until sharp LEED patterns were observed as described in the preceding section. A fourth-order polynomial background has been subtracted from the spectra in order to remove any background resonance effects. This type of function was chosen as it gave the best fit at both low- and high-binding energies for all of the photon energies used. The labels *A*–*E* refer to the points at which the CIS spectra were constructed.

The main features of the valence bands of rutile and anatase single crystals have been discussed in detail elsewhere.[2,7,12] In all cases the valence band is around 6 eV wide. The states to low-binding energy (around 5 eV BE) have been assigned mainly to Ti 3*d*-O 2*p* π-bonding states, while at higher binding energy (around 8 eV BE), states arising predominantly from O 2*p*-Ti 3*d* σ-bonding are found.[2,3,30] A defect peak due to reduced Ti^{3+} (*D*) is observed at around 1 eV BE. Figure 2 reveals significant differences between the three surfaces. First, while the valence-band spectra of both anatase surfaces show two main features (at around 5 and 8 eV BE), the structure observed for rutile is more complex. Secondly, there are strong variations in the intensity of the defect peak *D* with the contrast between the

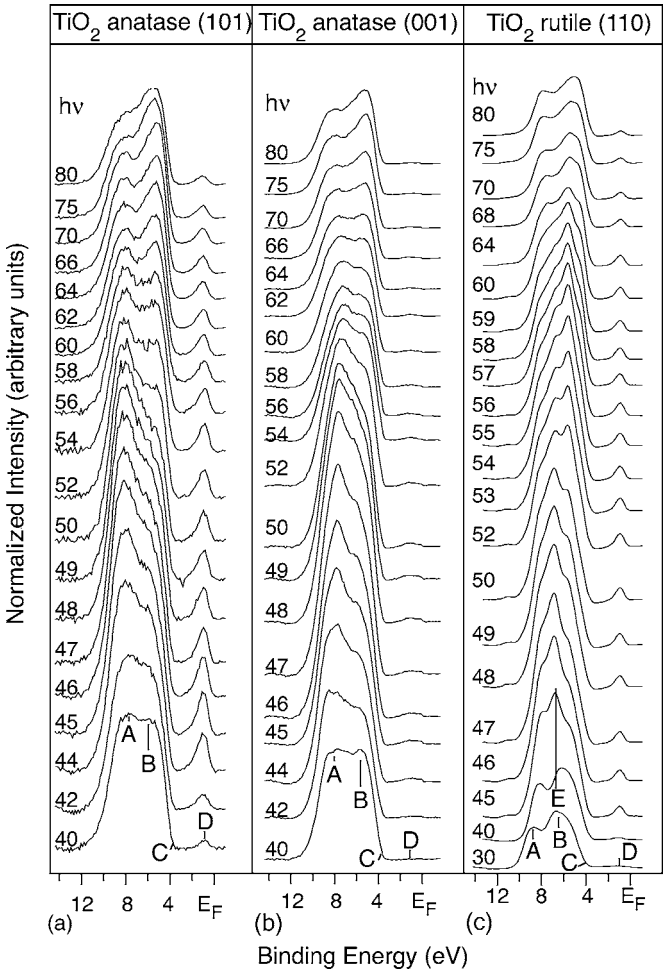

FIG. 2. EDC spectra of TiO_2 surfaces (a) anatase (101), (b) anatase (001), and (c) rutile (110) recorded at normal emission. The method of preparation for these surfaces is described in the text. The spectral intensity is normalized to the incident photon flux. All spectra are aligned on the binding-energy scale to a Fermi edge recorded from a Ta clip holding the samples in place and a fourth-order polynomial background has been subtracted. Points *A*–*E* refer to the binding energies at which CIS spectra were reconstructed (see the text).

(101) and (001) anatase surfaces being particularly marked. Figure 2 also shows the intensity variation of the spectra on moving through the Ti 3*p* resonance threshold (the onset of which is at the 3*p*-3*d* threshold at around 47 eV). For the anatase surfaces, an increase in relative intensity of the lower binding energy feature (marked *A*) at around 8 eV is clearly seen on resonance. For the rutile (110) surface a similar effect is observed, masked in this case by the increased complexity of the valence-band features. These effects are discussed in more detail below.

2. Valence-band photoemission: Rutile (110) surface

At photon energies well removed from resonance, the valence band of the rutile (110) surface shows two main peaks at binding energies of around 5.8 and 8.2 eV. At intermediate energies a further large peak (the so-called "overlap peak,"[2] marked *E*) is observed at a binding energy of 6.7 eV, to-

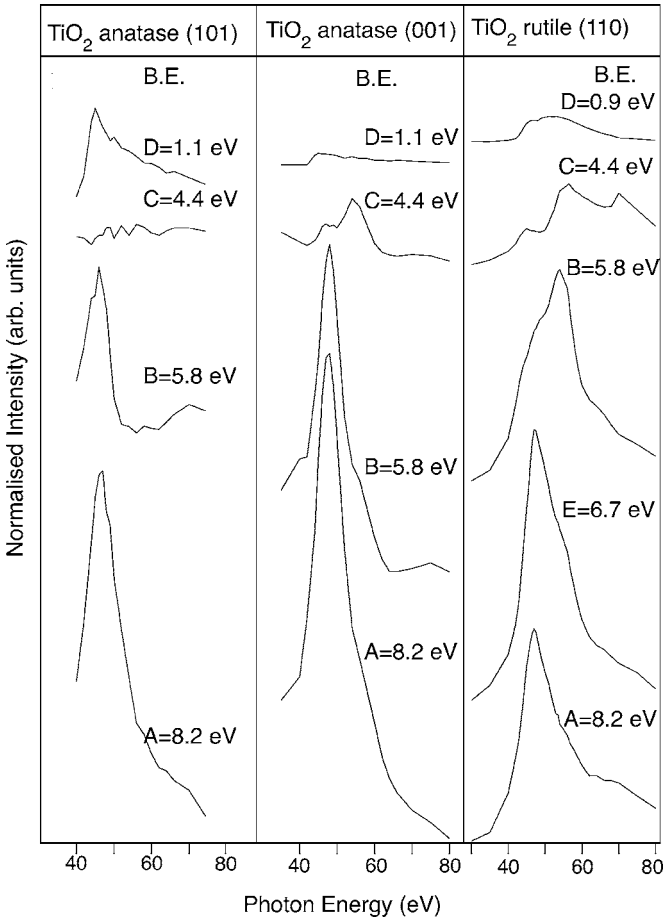

FIG. 3. CIS spectra constructed from the EDCs in Fig. 2. The CIS spectra were constructed by taking the intensity of the EDCs at the fixed binding energies indicated.

gether with a shoulder on the low-binding energy side of the valence band at photon energies in the range 54–75 eV. A clear feature due to the defect state is observed at 1.1 eV.[2,3,5] Our data bear a close resemblance to those recorded by Nerlov *et al.*,[3] particularly following the creation of surface defects.

The resonance CIS spectra of rutile in Fig. 3 show a resonance at 47 eV over all 3 of the main valence-band peaks (*A*, *B* and *E*) indicating 3*d* character throughout the valence band in agreement with previous work.[2,7] A significant resonance at an energy of 54 eV is also observed, particularly for peak *B*, where the 54 eV resonance dominates the spectrum. Here, a smaller resonance is observed at a photon energy of 47 eV. Overall, these resonances are in agreement with previous studies of the rutile (110) surface.[2,3] The energy difference between these two resonance peaks is approximately equal to the energy difference between the Ti 3*d* and Ti 4*sp* orbitals in TiO_2.[2,31,32] Since the Ti 4*sp* states are strongly hybridized with the O 2*p* valence-band states, particularly at the surface,[2] we can assign the resonance at 54 eV to a Ti 3*p*-Ti 4*sp*/O 2*p* interatomic resonance process. The CIS spectra recorded from the VBM for rutile (marked *C* in Figs. 2 and 3) again show a broad resonance with a main component at 54 eV indicating a dominant contribution from Ti 4*sp* states in this part of the valence band. Peak *D*, arising from Ti^{3+} states (d^1) is also seen to resonate at 46 and 53 eV. We note that the Ti 4*sp* resonance is very slightly stronger than the Ti 3*d* resonance, whereas in the work of Zhang *et al.*[2] the Ti 3*d* resonance is slightly stronger. The surface defect density is similar in both cases—a measure of this, for example, is the ratio of the height of the defect state peak to the height of the low-binding energy (5.8 eV) valence-band peak. This is 0.11 in the present work and 0.09 in the work of Zhang *et al.*[2] The reason for this difference is thus unclear but it may lie in the history of the crystals, in particular, the bulk defect density.[5] We should also note that the data presented in this work were recorded at normal emission with angular resolution, whereas those in Ref. 2 are recorded using a cylindrical mirror analyzer (CMA), which means that they are partially angle-integrated spectra. This may account for the differences in the appearance of the spectra. The effect of processing history on the appearance of the spectra is discussed further in Sec. III B.

Overall, the CIS spectra for rutile agree well with site-specific x-ray photoelectron spectroscopy (XPS) and associated *ab initio* local density approximation (LDA) plane-wave basis-set calculations for rutile (110),[7] which show that there is a Ti contribution to the predominantly O 2*p* valence band with contributions from Ti 3*d* and 4*sp* states and some contribution from O 2*s* states. Figure 4(a) shows a simplified MO diagram indicating contributions from Ti 3*d*, 4*s*, 4*p*, and O 2*p* states to the rutile valence band, along with the *ab initio* LDA plane-wave basis set partial density-of-states (pDOS) calculations of Ref. 7. The Ti contribution is found to consist of a two-peaked structure arising from the σ and π splitting of the bonding states. The σ orbitals, corresponding to the high-binding energy part of the valence band (feature *A* in Fig. 2), have bonding contributions from Ti 4*sp* [to give a_{1g} (σ^b) molecular orbitals], Ti $3d_{x^2-y^2}$ and $3d_{z^2}$ [to form e_g (σ^b)], and Ti 4*p* [to give t_{1u} (σ^b)]. The Ti 4*p* orbitals also bond with ligand *p* orbitals [to give $t_{1u}(\pi^b)$] together with the Ti $3d_{xy}$, $3d_{xz}$, and $3d_{yz}$ [which form $t_{2g}(\pi^b)$]. In rutile, these form the central lobe of the valence band (feature *E* in Fig. 2) with some overlap with the lowest binding-energy lobe. The lowest energy part of the valence band (feature *B* in Fig. 2) is predominantly formed from the nonbonding t_{1g} and t_{2u} ligand orbitals, with some Ti 3*d* and 4*p* π character.

3. Valence-band photoemission: Anatase (101) and (001) surfaces

The anatase EDCs in Fig. 2 have been discussed fully elsewhere.[12] Here we will point out only the main features. Overall, the spectra are similar to those recorded from the rutile single crystal in that the valence band is around 6 eV wide, and there is a clear feature related to the defect state at around 1 eV binding energy. The spectra also show a clear Ti 3*p*-3*d* resonance at around 47 eV for the major valence-band peaks *A* and *B* and at the VBM, *C* and 46 eV for the defect state *D*. The CIS spectra in Fig. 3 for the two anatase surfaces indicate contributions from Ti 3*d* states for both of the major valence-band peaks (labeled *A* and *B* in Fig. 2) as indicated by the large resonances at 47 eV. In the case of the (101) surface, feature *A* at a binding energy of 8.2 eV shows a high-photon energy tail with some intensity at a photon energy $h\nu$, of around 54 eV. As described above for the

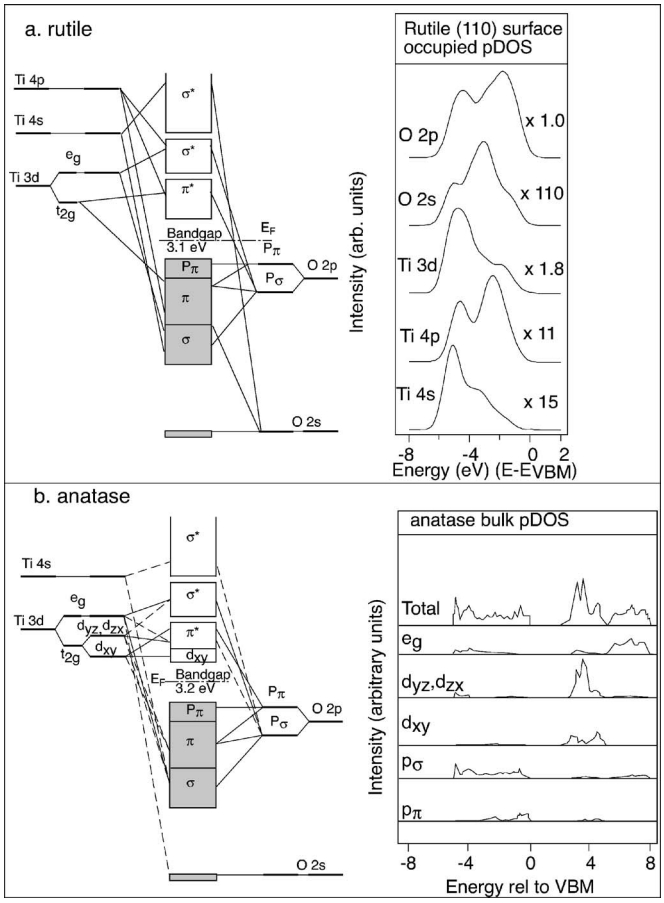

FIG. 4. Schematic molecular orbital diagrams for (a) rutile TiO_2, constructed from Ref. 7 with the corresponding *ab initio* LDA plane-wave basis-set pDOS calculations for the rutile (110) surface shown in the upper right panel [broadened with a 0.4 eV Gaussian curve (Ref. 7)] and (b) anatase TiO_2 adapted from Ref. 33 with the corresponding FLAPW pDOS calculations for bulk anatase shown in the lower right panel.

rutile (110) surface, this is attributed to Ti $3p \rightarrow 4sp$ resonance processes occurring through O $2p$-Ti $4sp$ hybridization in the valence band since the Ti $4sp$ states are thought to lie around 8 eV above the Ti $3d$ states.[2,3] Clearly, curve *B* for the anatase (101) surface shows there is little intensity around 54 eV suggesting that the valence band here contains only Ti $3d$ derived states. Feature *C* appears to show no structure either at 47 or 54 eV photon energy, suggesting the degree of O $2p$/Ti $3d$ and O $2p$/Ti $4sp$ hybridization in this part of the valence band is minimal. This is in agreement with BULK electronic structure calculations for anatase illustrated in Fig. 4(b);[33] no SURFACE calculations for anatase (101) have so far been published. The main difference between anatase and rutile revealed by bulk calculations is that the d_{xy} state in anatase is predicted to be effectively nonbonding and quite isolated, lying at the bottom of the conduction band [as illustrated in Fig. 4(b)], with corresponding nonbonding O $2p$ orbitals at the top of the valence band. This arises from structural differences between the two polymorphs; the local structure of rutile is more regular, with shorter metal-metal bond distances and the oxide is more dense than anatase. The lack of structure at feature *C* for the (101) surface is consistent with more O $2p$ nonbonding character at the VBM for anatase than for rutile, and in turn implies that the (101) surface is bulk terminated, in agreement with LEED for this surface. It is clear that the main contribution to this state comes from Ti $3d$ states, in contrast to the spectra from the rutile (110) surface.

In contrast to the (101) surface, CIS for the (001) surface (Fig. 3) shows significant intensity in peak *B* (BE=5.8 eV) at around $h\nu$=54 eV, suggesting that the (1×4) reconstruction [Fig. 1(c)] leads to a modification of Ti-O hybridization as discussed in our earlier work.[12] For both anatase surfaces the Ti $3p$-$3d$ resonance of the 8.2 eV BE peak is larger than that at 5.8 eV, suggesting stronger Ti $3d$-O $2p$ hybridization in the higher binding-energy part of the valence band. This is consistent with the calculations of Asahi *et al.* for bulk anatase, where Ti e_g states are shown to contribute strongly to the high binding-energy part of the valence band (σ-bonding interactions),[33] with only a small contribution from the t_{2g}, d_{yz}, and d_{zx} orbitals (π-bonding interactions). This is generally consistent with our expectations from molecular orbital theory, i.e., σ-bonding interactions are found at a higher binding energy than the weaker π-bonding interactions. In contrast to the (101) surface, a clear resonance at the VBM (*C* in Fig. 2) is observed with a maximum resonance intensity at 54 eV. This is assigned to Ti $4sp$ states contributing to the valence band. In addition, a smaller resonance is observed at a photon energy of 47 eV, indicating a smaller Ti $3d$ contribution.

4. Comparison of valence-band photoemission from rutile (110), anatase (101), and anatase (001) TiO_2 *surfaces*

The VBM occurs at 3.0 eV BE for all surfaces, which is consistent with the Fermi level being pinned close to the bottom of the conduction band. (The position of the VBM is determined using the approach described in Ref. 55.) There is a small difference in the binding energy of the feature associated with the defect state, which is seen in anatase at 1.1 eV compared to 0.9 eV in rutile (110). On comparing the photoemission spectra for the different surfaces, it is clear, however, that there are marked differences in defect concentration, and in Ti-O hybridization. The size of the feature arising from the defect state at a binding energy of around 1 eV varies markedly between the samples due to differences in the number of surface O vacancies, despite the fact that the same preparation method was used for all three surfaces shown in Figs. 1, 2, and 5–7. In the (001) crystal the peak is particularly weak, which we have previously linked to the (1×4) reconstruction of this surface.[12] This earlier work indicated that the (001) surface was particularly resistant to defect creation.[12] More recent density functional theory-generalized gradient approximation (DFT-GGA) calculations of rutile (110) and (001) and anatase (001) and (100) surfaces appear to support this experimental evidence, suggesting the (001) surface is more difficult to reduce.[34]

By comparison of the peak areas in the Ti $3p$ spectra shown in Fig. 5 (and discussed further in Sec. III A 5 below) we are able to estimate the O-vacancy concentration for each of the surfaces. We obtain values of 15 ± 2 %, 2 ± 2 %, and 8 ± 2 % Ti^{3+} for the anatase (101), (001), and rutile (110)

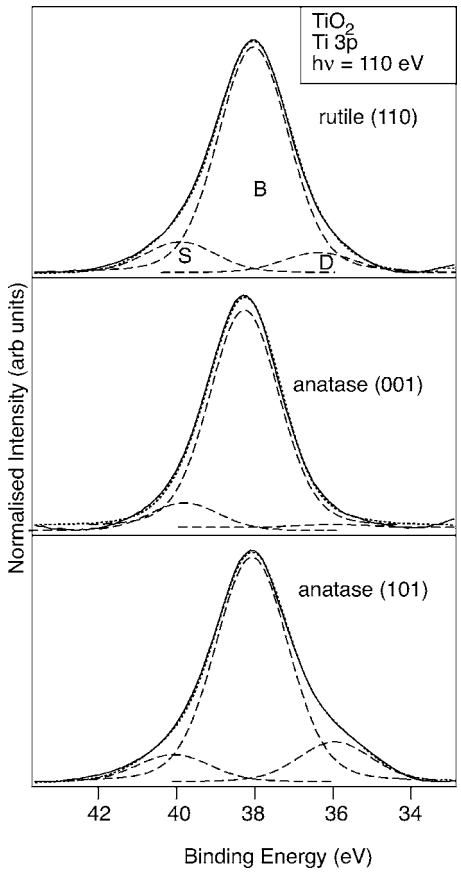

FIG. 5. Ti 3*p* spectra recorded at 110 eV photon energy. The spectra have been background subtracted and aligned on the binding-energy scale relative to a Fermi edge recorded from a clean Pt foil attached to the sample plate. The spectral intensity is normalized to the incident photon flux. The peak has been fitted with three Voigt functions of 85:15 Gaussian:Lorentzian weighting and equal FWHM. *B* is the bulk contribution, *D* arises from Ti^{3+} (see text), and we tentatively assign *S* to adsorbed surface hydroxyl groups.

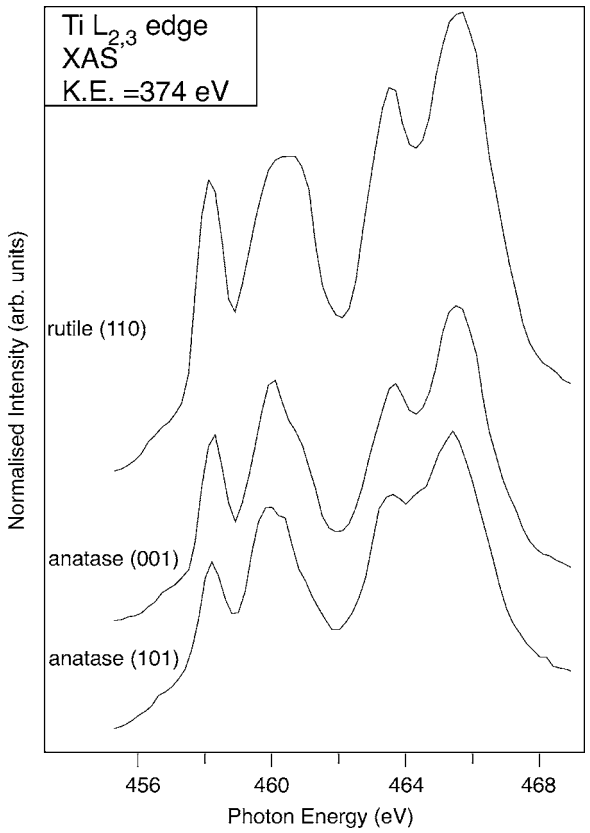

FIG. 6. XAS spectra recorded using Auger electron-yield detection from the Ti $L_{2,3}$ edges of TiO_2 anatase (101) and (001) and rutile (110) single-crystal surfaces. The spectral intensity is normalized to the incident photon flux. Photon-energy calibration was performed by means of a TiO_2 paste sample mounted adjacent to the incident-beam intensity monitor.

surfaces, respectively. As one oxygen vacancy gives rise to two Ti^{3+} ions, the estimated O-vacancy concentrations are 7 ± 2 %, 1 ± 2 %, and 4 ± 2 % for the (101), (001), and (110) surfaces, respectively. In the case of rutile this correlates well with the work of Wendt *et al.*,[16] where around 3% bridging O vacancies would be predicted for the sample processing conditions used in this work. The ratios between the defect-peak intensity and the intensity maximum of the valence band at 47 eV photon energy (Fig. 2) are 0.16, 0.02, and 0.07 for the anatase (101), (001), and rutile (110) surfaces, respectively, an ordering which correlates well with the relative proportions of oxygen vacancies at the different surfaces. Of the two anatase surfaces the (101) surface is the more stable surface, with lower surface energy.[35] Since it is now considered that O-vacancy sites are the active sites for many catalytic reactions on TiO_2 surfaces[5,17,36] the increased concentration of vacancies on the (101) surface relative to the anatase (001) and rutile (110) surfaces would appear to agree with the increased catalytic activity of anatase compared with rutile, assuming the predominant surface exposed in particulate samples is the lowest-energy (101) surface.

Although we observe contributions from nominally unoccupied Ti 3*d* and 4*sp* states for all three surfaces, it is clear that the distribution of these states within the valence band varies appreciably between the three samples. The differences in Ti-O hybridization between surfaces are evident, for example, at the low-binding energy side of the valence band (marked *C* in Fig. 2). For both the rutile (110) and anatase (001) surfaces, Ti resonances at 3*d* and 4*sp* energies are observed, the strongest being to the 4*sp* level. In contrast, only a very weak resonance is observed for the anatase (101) surface. 4*sp* resonances of varying intensities are also observed for the π-bonding part (line *B* in Fig. 3) of the valence band; this is particularly strong in the case of rutile. This is in agreement with the calculated pDOS of Woicik *et al.* for rutile where the 4*p* states are shown to contribute most strongly to the π-bonding part of the valence band.[7] While 3*p*-4*p* transitions are forbidden by the dipole selection rule, 3*p*-4*s* transitions are allowed, and in a noncentrosymmetric environment (such as a surface), *sp* mixing will lead to the inclusion of the 4*p* states in the resonance process. The differences between the CIS spectra at point *C* for the rutile (110) and anatase (101) surfaces are as predicted by bulk calculations for rutile and anatase[7,33,37] These indicate that there is a strong Ti 4*p* contribution to the states at the VBM in rutile[7] that is absent in anatase.[37] However, this does not

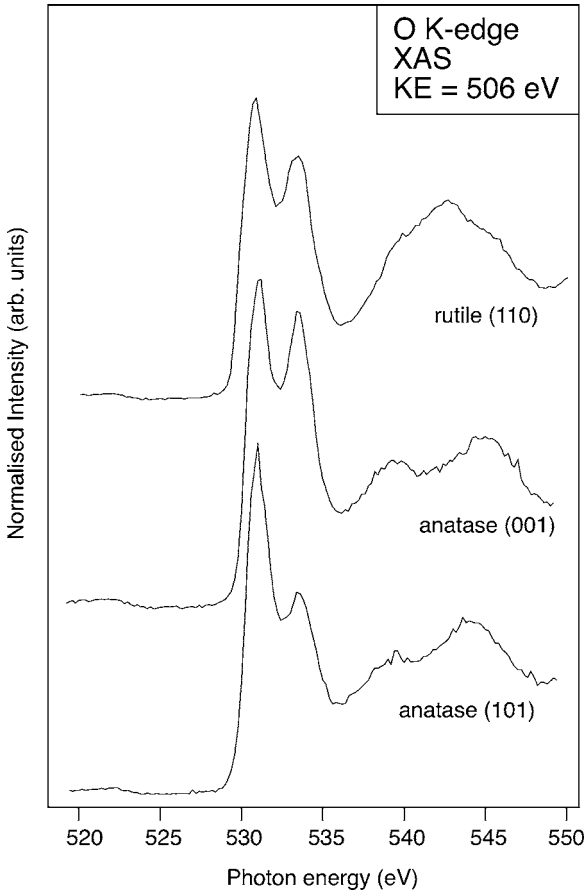

FIG. 7. XAS spectra recorded using Auger electron-yield detection from the O K-edge of TiO_2 anatase (101) and (001) and rutile (110) single-crystal surfaces. The spectral intensity is normalized to the incident-photon flux. Photon-energy calibration was performed by means of a TiO_2 paste sample mounted adjacent to the incident-beam intensity monitor.

explain why the anatase (001) surface shows appreciable 4*sp* character at point *C* in the valence band. We attribute this to the (1×4) reconstruction of the (001) surface, which leads to substantial surface microfacetting. We envisage that the resulting reduction in site symmetry of the Ti^{4+} ions may lead to substantial Ti 4*sp* hybridization at the surface that is not present in the bulk.

In all three samples, peak *D*, recorded from the defect state, shows a resonance at around 46 eV. The apparent variations in the intensity of the resonance are related to the defect concentrations on each of the surfaces. In all cases the percentage increase in intensity of the defect-state resonance between spectra recorded at 40 and 47 eV lies between 80 and 90%. The lower resonance energy observed for the defect state is due to the fact that this peak arises from reduced Ti^{3+} at the surface. This correlation between oxidation state and resonance onset energy has been observed in other mixed valency systems.[38] It appears that both the anatase (101) and rutile (110) defect-state resonances also show some contribution from Ti 4*sp* states, though the low-signal intensity makes this conclusion tentative.

5. Ti 3*p* core-level photoemission from rutile (110), anatase (101), and anatase (001) TiO_2 surfaces

Figure 5 shows Ti 3*p* spectra recorded at a photon energy of 110 eV. The spectra are background subtracted using a fourth-order polynomial and have been fitted with three Voigt curves of 85:15 Gaussian:Lorentzian weighting [labeled *S*, *B*, and *D* for the (101) surface]. The peak *B* originates from Ti^{4+} in the bulk of the sample and *D* from the presence of Ti^{3+}.[39] As described in the previous section, the relative intensities of peak *D* are in agreement with those of the defect state peak seen in the valence-band photoemission spectra. The surface region O-vacancy concentrations are estimated from Fig. 5 to be 15 ± 2 %, 2 ± 2 %, and 8 ± 2 % Ti^{3+} for the anatase (101), (001), and rutile (110) surfaces, respectively. The (001) surface shows the smallest peak associated with Ti^{3+}, further confirming its stability to the thermal production of O vacancies.

The origin of the peak labeled *S*, which has a similar intensity on all three surfaces, is unclear.[39] It has been suggested that the peak arises from the very topmost surface Ti ions with the shift to higher-binding energy occurring due to the reduced coordination of some of the surface Ti ions.[39] However, it was found that adsorption of water on rutile surfaces resulted in no change in the intensity of the feature.[39] It has also been suggested that this feature is a satellite,[39] though ELS measurements on unreduced rutile show no energy losses below 5 eV that could give rise to it.[17,40,41] ELS studies of rutile TiO_2 with O vacancies show a loss peak at around 1.3–1.9 eV energy loss,[17,40,41] which has been ascribed to a polaronic excitation associated with the Ti^{3+} d^1 configuration.[41] It is not possible that peak *S* is a satellite associated with this loss as it occurs at a binding energy of 2 eV above the main peak, *B*. Such a satellite-loss peak would be expected to lie around 1.3–1.9 eV to high-binding energy of the defect peak *D* (as it is associated with the presence of Ti^{3+}). Following adsorption of bi-isonicotinic acid (BINA) on the surfaces of rutile or anatase, it is seen that both peaks *D* and *S* decrease in intensity relative to the main peak *B*,[42] suggesting that this peak arises from the topmost surface layers. In the light of recent STM studies of rutile (110) surfaces,[16] it is possible that this peak arises from the formation of surface Ti-OH species. Wendt *et al.* have recently discovered that even at pressures of 10^{-11} Torr, clean rutile surfaces become contaminated with OH via adsorption of water from the background vacuum.[16] This reaction takes place predominantly at oxygen vacancy sites,[43] and under typical UHV conditions, results in partial occupancy of these sites by OH species.[16] Although, to the authors' knowledge, no XPS data exist for well-defined Ti hydroxides, in the cases of $Cr(OH)_3$, Mn(OH)O, and $Ni(OH)_2$ the metal 2*p* or 3*p* core level is shifted by around 1 eV to higher-binding energy relative to Cr_2O_3, Mn_2O_3, and NiO, respectively.[44–47] As mentioned above, adsorption of BINA results in a decrease in the intensity of this peak,[42] which could occur as OH is displaced in favor of the carboxylic acid. Assignment of this peak to Ti-OH would also explain why adsorption of water does not result in a change in the peak intensity, assuming the surface is already saturated with OH species. We thus tentatively suggest that peak *S* may be assigned to surface Ti-OH species.

6. Ti L-edge (2p) and O K-edge (1s) XAS from rutile (110), anatase (101), and anatase (001) TiO_2 *surfaces*

Figure 6 shows XAS spectra at the Ti L edge ($2p$) for the three samples recorded in constant final state (CFS) mode using a fixed hemispherical analyzer set to collect Ti LMV Auger electrons at a kinetic energy of 374 eV. The spectra are in excellent agreement with similar XAS and electron energy loss (ELS) data recorded from polycrystalline films and naturally occurring single crystals, and with calculated XAS spectra.[31,32,48–50] For all three samples two sets of peaks separated by 6 eV are clearly seen. This splitting arises from the core-hole spin-orbit splitting of the $2p$ levels.[31,48] The structure within these two sets of peaks is believed to arise from the crystal-field splitting of the d-derived final states into t_{2g}- and e_g-like levels.[31,48–50] The main difference in the Ti $2p$ absorption spectra between the rutile and anatase crystals occurs in the double-peaked feature at around 460 eV photon energy, with a change in the relative intensity of the two peaks. In rutile the peaks are of the same intensity, whereas in anatase the lower photon-energy peak has greater intensity. Between the two anatase surfaces there is a slight difference in the relative intensities of the two peaks centered around 460 eV photon energy. A number of explanations have been put forward for this splitting, including splitting of the e_g state due to reduction of local-site symmetry from octahedral[31,32] and a dynamic Jahn-Teller effect, where the electronic and vibrational states couple in the excited state.[31] Calculations using the local-site atomic positions, however, fail to reproduce the splitting, suggesting that longer-range interactions may play a part in the splitting.[50] Since our spectra are recorded in Auger yield mode, i.e., electron emission, they are surface sensitive and we would expect the different surface structures to give rise to variations in the peak at $h\nu$=460 eV if, as Ruus *et al.* suggest, the local environment around the absorbing atom plays a significant role.[49] It is can also be seen that the intensity of the transition to the e_g-derived final state varies with the surface and is strongest for the anatase (101) surface. This is discussed further below.

The O $1s$ XAS shown in Fig. 7 are also in good agreement with previous work recorded from polycrystalline thin films and natural single crystals. Again, the spectra are recorded in Auger yield mode monitoring the emission of O KLL Auger electrons with KE=506 eV. The two sharp peaks at photon energies of 531 and 533 eV are attributed to excitations into the Ti $3d$ t_{2g} and e_g levels, respectively.[31,49] The structure at higher energy arises from delocalized states derived from the antibonding Ti $4sp$/O $2p$ band.[49] Excitations to Ti $3d$-derived unoccupied states from O $1s$ must occur due to strong hybridization between the O $2p$ and Ti $3d$ states, giving these states an element of O $2p$ character. O $1s$ XAS is thus a particularly sensitive probe of the extent of hybridization between O and Ti states. The e_g feature corresponds to the σ-antibonding part of the interaction between O $2p$ and Ti $3d$ e_g orbitals, whereas the t_{2g} feature corresponds to the weaker π-antibonding part of the interaction. It is therefore interesting to note the marked variations in the relative intensities of the t_{2g} and e_g features with the surface probed. The e_g feature at 533 eV photon intensity is markedly less intense than the t_{2g} feature (at 531 eV) in the case of anatase (101) [and to some extent rutile (110)]. In the case of the anatase (001) surface, the features have comparable intensity. This leads us to conclude that the Ti $3d$ e_g-O $2p$ hybridization influencing the intensity of this feature is weaker in the case of the anatase (101) surface than for the (001) surface. This would in turn imply that the σ-antibonding "e_g" state should have stronger Ti $3d$ character at the anatase (101) surface than at the (001) face. This can be seen directly in Fig. 6, where the Ti $3d$ character of the states is probed through excitation at the Ti $L_{2,3}$ edge. Here we find that the intensity ratio between the e_g feature at 460 eV photon energy and the t_{2g} feature at around 458 eV photon energy is larger for the anatase (101) surface than for the (001) plane.

Given the surface-sensitive nature of the partial electron-yield detection used, it seems likely that the reduction in Ti $3d$-O $2p$ hybridization in these e_g states is due to the presence of a large concentration of oxygen vacancies at the (101) surface; indeed, we note from the comparison of Fig. 7 with Fig. 2 that the intensity of the e_g feature at the O K edge increases as the number of surface-oxygen vacancies is reduced. In the case of rutile (110) it is well established that the oxygen ions removed on argon ion bombardment are the twofold-coordinated "bridging" oxygen ions, which bridge between approximately octahedrally coordinated Ti ions in the second layer[5,17] [Fig. 1(a)]. The rutile (110) and anatase (101) surface are crystallographically equivalent, and the topmost layer of the anatase (101) surface also consists of rows of twofold-coordinated oxygen atoms[13] [Fig. 1(b)]. We might reasonably expect these to be removed by argon-ion bombardment. Removal of each of these ions removes two Ti-O σ bonds from adjacent Ti-O_6 octahedra, each locally involving an O $2p$ orbital and an e_g orbital of Ti, and so would be expected to reduce the O $2p$ character of the mainly Ti $3d$ σ-antibonding e_g states, as is observed.

One might expect that this should also be reflected in the atomic parentage of the filled states probed by photoemission. However, while the XAS measurements are sensitive to the Ti pDOS in the empty states, and are thus a good probe of changes in the strong Ti $3d$ e_g-O $2p$ σ interaction, the photoemission measurement probes the filled DOS, which consists of states of mainly O $2p$ character, with a small admixture of Ti $3d$ and $4sp$. The σ-bonding part of the Ti $3d$ e_g-O $2p$ interaction is contained within the feature at around 8 eV binding energy (feature A) of Fig. 2. However, band-structure calculations for anatase (101) suggest that this part of the valence band also contains features arising from the π-bonding interaction between Ti $3d$ d_{yz} and d_{zx} and O $2p$,[33] with the feature at around 6 eV (feature B) showing only a small amount of t_{2g} character. Thus there is no distinct part of the valence band associated only with the O $2p$-Ti $3d$ e_g σ-bonding interaction. The photoemission measurements are, however, sensitive in other ways to the removal of surface oxygen, and reveal changes in the O $2p$-Ti $3d$ t_{2g} π-bonding interaction with surface-defect concentration, as we discuss in Sec. III B.

B. Effect of preparation method/sample history on the anatase (101) valence-band electronic structure

The effect of exposure to O_2 and annealing temperature on the atomic character of the valence-band states of the

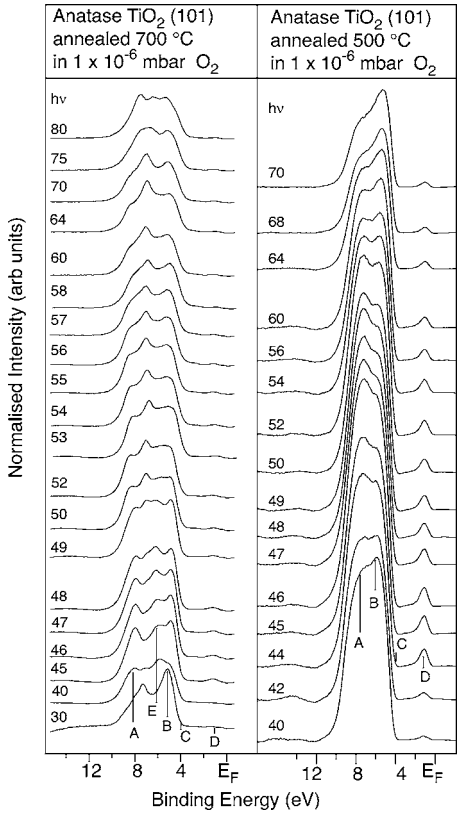

FIG. 8. Comparison of the EDCs of anatase (101) following annealing in O_2 at 700 °C (left-hand panel) and annealing in O_2 at 500 °C (right-hand panel). The spectral intensity is normalized to the incident-photon flux, and spectra are recorded at normal emission. All spectra are aligned on the binding-energy scale to a Fermi edge recorded from a Ta clip holding the samples in place and have had a fourth-order polynomial background subtracted. Points *A–E* refer to the binding energies at which CIS spectra were reconstructed (see the text).

anatase (101) surface has been investigated. Figure 8 shows EDC spectra for two different surface-preparation methods of the anatase (101) surface. In the first, the (1×1) surface was sputtered and annealed to obtain a LEED pattern as described above followed by annealing in 1×10^{-6} mbar O_2 for 15 min at 700 °C. No surface contamination could be detected in Auger spectra. The second method involved sputtering the sample until no surface-carbon contamination could be detected in Auger spectra and then annealing at 500 °C in 1×10^{-6} mbar O_2 for 20 min. A LEED pattern could not be obtained following this latter treatment. Again a fourth-order polynomial background has been subtracted from the EDCs. Both data sets show a reduction in the intensity of the defect state compared to the spectra in Fig. 2, due to oxidation of Ti^{3+} to Ti^{4+}, with the change being substantial in the higher-temperature annealed sample. For the low-temperature annealed sample there is very little obvious change in the main valence-band structure compared to the sample annealed in a vacuum to produce a (1×1) LEED pattern (and shown in Fig. 2), except for the reduction in defect-state intensity. However, the corresponding CIS spectra in Fig. 8 (right-hand panel) do show some changes, mainly in that there now appears to be a contribution from 4*sp* states throughout the valence band. In the 700 °C annealed sample the effect is more dramatic. The feature arising from the defect-state peak is strongly reduced in intensity. The main valence band now shows a three-peaked structure similar to that recorded from rutile (110) shown in Fig. 2. As discussed earlier, in the case of rutile (110), the central lobe of the valence band (the "overlap" peak at around 6.7 eV BE) has predominantly O 2*p* character, mixed mainly with Ti 3*d* t_{2g} orbitals and a small element of Ti 4*sp* character. This is clearly severely attenuated by the removal of surface oxygen, as illustrated in Fig. 8. The CIS spectra for this sample also show some changes compared with the vacuum-annealed anatase (101) surface shown in Fig. 3. The π-derived band (low-binding energy side of the valence band, *B*) and the "overlap" peak [*E*, between the σ-(*A*) and mainly π-(*B*) derived peaks] both show a resonance at around 54 eV, i.e., there is now a Ti 4*sp* contribution to these parts of the valence band. There is a larger contribution to the VBM (*C*) and to feature *B* from both Ti 3*d* and 4*sp* states than in the vacuum-annealed sample (Fig. 2). The CIS data therefore indicate that the extent of 4*sp* and 3*d* mixing in the π-bonding parts of the anatase (101) surface decreases with increasing oxygen-vacancy concentration (correlating with our observations from the EDCs above). We note that a high degree of 4*sp* mixing at low-defect concentration was also observed for the anatase (001) surface shown in Fig. 3.

C. Correlation between electronic structure and reactivity of TiO_2 surfaces

Although TiO_2 is widely used for photocatalytic oxidation (for example, the breakdown of organic pollutants in aqueous solution), the detailed mechanism is not completely clear.[1] Following the absorption of a photon, the holes created in the valence band are believed to form hydroxyl radicals $(\text{-}Ti^{IV}OH^{\cdot})^{+}$ by reaction with surface titanol $(\text{-}Ti^{IV}OH)$ groups, which may act to oxidize organic species. Meanwhile, the electron created in the conduction band reacts with O_2 to form an effective oxygenation agent, superoxide (O_2^-), in a rate-limiting step, which also scavenges excess photoexcited electrons.[1,17] This process is thought to occur by initial dynamic trapping of the conduction-band electron in shallow traps at surface titanol groups to form $\text{-}Ti^{III}OH$ groups, which then react with O_2 to reoxidize the titanol groups to $\text{-}Ti^{IV}OH$. Thus, both the electron and the hole created by photoexcitation are believed to act via surface titanol groups, in the case of the electron, via surface reduction to a state very similar to the defect state created by oxygen loss.[17] In terms of electronic structure, rapid transport of carriers and dynamic trapping at surface-defect sites would be aided by good overlap of the relevant wave functions. Thus it would be anticipated that strong mixing of Ti and O states at the conduction-band minimum and at the VBM, together with overlap of the latter with the defect state, would facilitate photooxidation.

It has long been established that TiO_2 surfaces containing O vacancies exhibit higher catalytic activity than defect-free surfaces to reactions such as dissociation of water.[17,36] It has also been established that the anatase phase of TiO_2 exhibits

higher reactivity than the rutile form, though mixtures of anatase powders with rutile powder show an increased rate of catalytic activity for some reactions.[51] The presence of O vacancies at TiO_2 surfaces leads to the formation of the band-gap state discussed above. A similar state has also been observed in several studies of photoexcited TiO_2 (Refs. 52–54) and studies of O_2-mediated dissociation of water at such sites have recently shown that these states play a major role.[17,43] In the case of the rutile (110) surface, it has been found that O_2 reacts with bridging OH groups formed as a result of water dissociation at oxygen-vacancy defects on the surface, confirming that the scavenging role of O_2 in photocatalysis involves a direct reaction between O_2 and trapped electrons located at bridging -Ti^{III}OH groups.[17]

Thus it seems clear that the photocatalytic activity of different surfaces will be influenced both by defect concentration and by the atomic makeup of the states close to the Fermi energy. The spectra of the three surfaces described in Sec. III A show that following identical surface preparations, the (101) anatase surface has the strongest defect-state intensity relative to the VBM. It also indicates that this state is mainly 3*d* in character with some 4*sp* character. The (001) surface shows a similar distribution of Ti-derived states although the concentration of defects is markedly lower and there is an increase in the concentration of 4*sp* states, particularly around the VBM. Anatase (101) is the most stable of the anatase surfaces[35] and is therefore expected to be the dominant exposed surface in powders used in catalytic reactions. The higher-defect density of the anatase (101) surface compared with the crystallographically equivalent rutile (110) surface correlates with the observed higher photocatalytic activity of anatase.[1] We predict the anatase (001) surface to be catalytically rather inactive. Our observations of a low-defect density on this surface are consistent with recent DFT-GGA calculations, which show a higher energy of formation of an oxygen-vacancy defect on anatase (001) than on rutile (110); a calculation for anatase (101) is not available.[34]

In terms of the atomic character of the states close to the Fermi energy, Fig. 3 shows that the anatase (101) surface is markedly different from anatase (001) or rutile (110) surfaces, in that it shows markedly less Ti 3*d* or 4*sp* character in the states around the VBM (points *B* and *C*). This in turn means that the "antibonding" part of this interaction (the states at the conduction-band minimum) should be of quite pure Ti 3*d* character with little mixing with O 2*p*. This runs counter to our assumption above that good mixing of these states should be important in photocatalytic activity, but it may lead to efficient localization of the conduction-band electron created on photoabsorption in a state of Ti^{III} character. It is also clear from our experiments that the atomic character of these states is itself a function of defect concentration. For the anatase (101) surface, reducing the concentration of defects leads to an increase in the contribution of 4*sp* and 3*d* states at the VBM and in the π-derived part of the valence band (feature *B* in Figs. 1 and 9). Clearly, for the O-annealed surfaces the overall concentration of surface O vacancies is reduced, and improved Ti-O hybridization would be expected. If photocatalytic activity is enhanced by increased defect concentration (corresponding in solution to increased bridging -Ti^{III}OH concentration)[17] and by good mixing between Ti and O states around the Fermi energy, then it can be seen that these effects act in opposition, in turn suggesting that there is an optimum defect concentration for activity in photocatalysis, above and below which activity should decrease. In this context it is interesting to note that in solution, an optimum dissolved oxygen content is observed for efficient photocatalysis over TiO_2.[1]

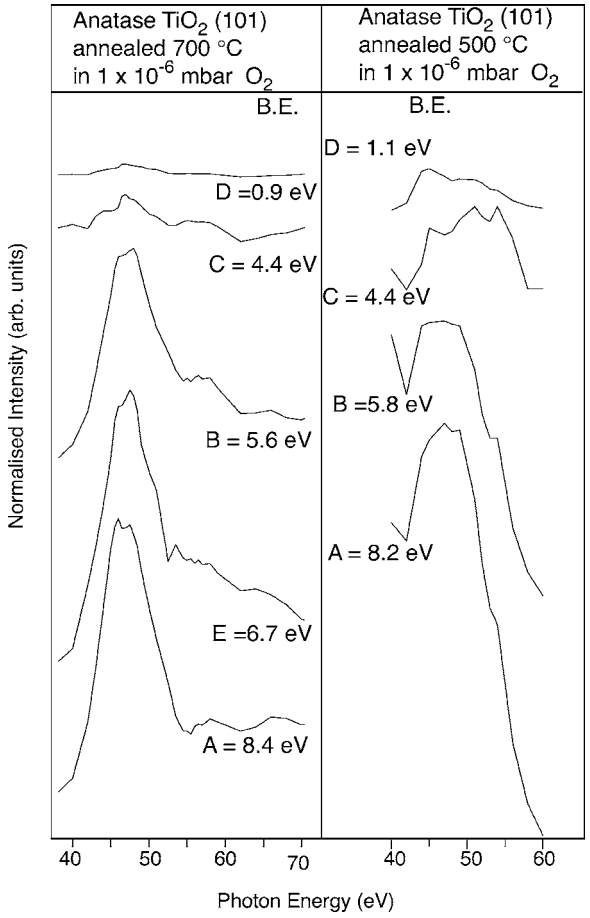

FIG. 9. Comparison of CIS spectra for anatase TiO_2 (101) annealed at 700 °C in O_2 and at 500 °C in O_2. The CIS spectra were constructed by taking the intensity of the EDCs at the fixed binding energies indicated.

IV. CONCLUSIONS

We have compared the electronic structure of anatase (101), anatase (001), and rutile (110) surfaces as a function of oxygen-defect concentration. For identically prepared surfaces, both the defect concentration and the atomic character of the states close to the Fermi energy is affected by the nature of the surface. Under the same conditions, the most stable anatase (101) surface shows the highest concentration of surface defects, consistent with the higher photocatalytic activity of anatase over rutile. In marked contrast, the anatase (001) surface shows a very low concentration of oxygen vacancies, consistent with earlier work.[12,14,21] We predict this surface to be rather catalytically inactive.

For these surfaces, prepared under identical cycles of bombarding and annealing *in vacuo*, we observe stronger mixing of Ti 3*d* states with O 2*p* in the mainly σ-bonding than in the π-bonding parts of the valence band, as would be expected from molecular-orbital theory. However, the anatase (101) surface shows rather lower Ti 3*d* character in the π-bonding part of the valence band than either rutile (110) or anatase (001), and for this surface the Ti 3*d* and 4*sp* mixing at the VBM is lower than for the other two surfaces.

We show that surface preparation and specifically O content play a large part in determining the atomic character of the states close to the Fermi energy. Using XAS, which is particularly sensitive to the Ti contributions to the DOS, we show that the strong Ti 3*d* e_g/O 2*p* σ-antibonding interaction is reduced as the number of oxygen vacancies increases. Photoemission, which is more sensitive to the O contributions, shows that as the number of surface defects is increased, the O 2*p*-Ti 3*d* t_{2g} π-bonding interaction is disrupted. In addition, the contribution of Ti 4*sp* and 3*d* states around the VBM decreases. This leads us to suggest that there is an optimum defect concentration for activity in photocatalysis, above and below which activity should decrease.

While some DFT-GGA calculations now exist for the anatase (001) surface,[34] similar calculations for the (101) surface are urgently required for comparison with this work.

ACKNOWLEDGMENTS

This work was funded by EPSRC (UK) under Grant No. GR/S07131, CCLRC, and the EU human mobility programme. G.C.S. and S.R. acknowledge CASE studentships from Johnson Matthey Plc. Thanks are also due to Michael Grätzel and his group at EPF Lausanne for supplying us with the anatase single crystals.

*Corresponding author. Electronic address: a.g.thomas@manchester.ac.uk

†Present address: CCLC Nantes Atlantique, Centre René Gauduchéau, Blvd. Prof. Jacques Monod, 44805 St. Herblain, France.

‡Present address: Synchrotron Soleil, L'Orme des Merisiers, Saint Aubin-BP 48, 91192 Gif sur Yvette, France.

§Present address: Laboratoire de Physico-Chimie des Surfaces, UMR 7045 ENSCP-CNRS, 11 rue Pierre et Marie Curie, F-75005 Paris, France.

[1] O. Carp, C. L. Huisman, and A. Reller, Prog. Solid State Chem. **32**, 33 (2004).

[2] Z. Zhang, S.-P. Jeng, and V. E. Henrich, Phys. Rev. B **43**, 12004 (1991).

[3] J. Nerlov, Q. Ge, and P. J. Møller, Surf. Sci. **348**, 28 (1996).

[4] R. Heise, R. Courths, and S. Witzel, Solid State Commun. **84**, 599 (1992).

[5] U. Diebold, Surf. Sci. Rep. **48**, 53 (2003).

[6] E. Bertel, R. Stockbauer, and T. E. Madey, Phys. Rev. B **27**, 1939 (1986); E. Bertel, R. Stockbauer, and T. E. Madey, Surf. Sci. **141**, 355 (1984).

[7] J. C. Woicik, E. J. Nelson, L. Kronik, M. Jain, J. R. Chelikowsky, D. Heskett, L. E. Berman, and G. S. Herman, Phys. Rev. Lett. **89**, 077401 (2002).

[8] P. W. Murray, F. M. Leibsle, C. A. Muryn, H. J. Fisher, C. F. J. Flipse, and G. Thornton, Surf. Sci. **321**, 217 (1994).

[9] P. J. Hardman, P. L. Wincott, G. Thornton, A. P. Kaduwela, and C. S. Fadley, Phys. Rev. B **60**, 11700 (1999).

[10] H. Raza, C. L. Pang, S. A. Haycock, and G. Thornton, Phys. Rev. Lett. **82**, 5265 (1999).

[11] G. Charlton, P. B. Howe, C. L. Nicklin, P. Steadman, J. S. G. Taylor, C. A. Muryn, S. P. Harte, J. Mercer, R. McGrath, D. Norman, T. S. Turner, and G. Thornton, Phys. Rev. Lett. **78**, 495 (1997).

[12] A. G. Thomas, W. R. Flavell, A. R. Kumarasinghe, A. K. Mallick, D. Tsoutsou, G. C. Smith, R. Stockbauer, S. Patel, M. Grätzel, and R. Hengerer, Phys. Rev. B **67**, 035110 (2003).

[13] W. Hebenstreit, N. Ruzycki, G. S. Herman, Y. Gao, and U. Diebold, Phys. Rev. B **62**, R16334 (2000).

[14] G. S. Herman, M. R. Sievers, and Y. Gao, Phys. Rev. Lett. **84**, 3354 (2000).

[15] L. Kavan, M. Grätzel, S. E. Gilbert, C. Klemenz, and H. J. Scheel, J. Am. Chem. Soc. **118**, 6716 (1996).

[16] S. Wendt, J. Matthiesen, R. Schaub, E. K. Vestergaard, E. Lægsgaard, F. Besenbacher, and B. Hammer, Phys. Rev. Lett. **96**, 066107 (2006).

[17] M. A. Henderson, W. S. Epling, C. H. F. Peden, and C. L. Perkins, J. Phys. Chem. B **107**, 534 (2003).

[18] L. C. Davies, J. Appl. Phys. **59**, R25 (1986).

[19] A. G. Thomas, W. R. Flavell, P. M. Dunwoody, C. E. J. Mitchell, S. Warren, S. C. Grice, P. G. D. Marr, D. E. Jewitt, N. Khan, V. R. Dhanak, D. Teehan, E. A. Seddon, K. Asai, Y. Koboyashi, and N. Yamada, J. Phys.: Condens. Matter **12**, 9259 (2000).

[20] W. R. Flavell, A. G. Thomas, D. Tsoutsou, A. K. Mallick, M. North, E. A. Seddon, C. Cacho, A. E. R. Malins, S. Patel, R. L. Stockbauer, R. L. Kurtz, P. T. Sprunger, S. N. Barilo, S. V. Shiryaev, and G. L. Bychkov, Phys. Rev. B **70**, 224427 (2004).

[21] Y. Liang, S. Gan, S. A. Chambers, and E. I. Altman, Phys. Rev. B **63**, 235402 (2001).

[22] M. Lazzeri and A. Selloni, Phys. Rev. Lett. **87**, 266105 (2001).

[23] R. E. Tanner, Y. Liang, and E. I. Altman, Surf. Sci. **506**, 251 (2002).

[24] P. Finetti, D. M. P. Holland, C. J. Latimer, C. Binns, F. M. Quinn, M. A. Bowler, and A. F. Grant, Nucl. Instrum. Methods Phys. Res. B **184**, 627 (2001).

[25] M. D. Roper and J. Purton, Nucl. Instrum. Methods Phys. Res. A **467**, 516 (2001).

[26] M. Bowler, J. B. West, F. M. Quinn, D. M. P. Holland, B. Fell, P. A. Hatherly, I. Humphrey, W. R. Flavell, and B. Hamilton, Surf. Rev. Lett. **9**, 577 (2002).

[27] Y.-L. Mathis, P. Roy, B. Tremblay, A. Nucara, S. Lupi, P. Calvani, and A. Gerschel, Phys. Rev. Lett. **80**, 1220 (1998).

[28] P. G. D. Marr, Ph.D. Thesis, UMIST, Manchester, UK, 2001.

[29] R. Hengerer, B. Bolliger, E. Erbudak, and M. Grätzel, Surf. Sci. **460**, 162 (2000).

[30] S. Munnix and M. Schmeits, Phys. Rev. B **30**, 2202 (1984).

[31] F. M. F. de Groot, M. Grioni, J. C. Fuggle, J. Ghijsen, G. A.

Sawatzky, and H. Petersen, Phys. Rev. B **40**, 5715 (1989).
[32] R. Brydson, H. Sauer, W. Engel, J. M. Thomas, E. Zeitler, N. Kosugi, and H. Kuroda, J. Phys.: Condens. Matter **1**, 797 (1989).
[33] R. Asahi, Y. Taga, W. Mannstadt, and A. J. Freeman, Phys. Rev. B **61**, 7459 (2000).
[34] A. Bouzoubaa, A. Markovits, M. Calatayud, and C. Minot, Surf. Sci. **583**, 107 (2005).
[35] M. Lazzeri, A. Vittadini, and A. Selloni, Phys. Rev. B **63**, 155409 (2001).
[36] I. M. Brookes, C. A. Muryn, and G. Thornton, Phys. Rev. Lett. **87**, 266103 (2001).
[37] C. Qiang and C. Hong-Hong, Chin. Phys. **13**, 2121 (2004).
[38] W. R. Flavell, J. Hollingworth, J. F. Howlett, A. G. Thomas, M. M. Sarker, S. Squire, Z. Hashim, M. Mian, P. L. Wincott, D. Teehan, S. Downes, and F. E. Hancock, J. Synchrotron Radiat. **2**, 264 (1995).
[39] P. J. Hardman, N. S. Prakash, C. A. Muryn, G. N. Raikar, A. G. Thomas, A. F. Prime, G. Thornton, and R. J. Blake, Phys. Rev. B **47**, 16056 (1993).
[40] W. Göpel, J. A. Anderson, D. Frankel, M. Jähnig, K. Phillips, J. Schafer, and G. Rocker, Surf. Sci. **139**, 333 (1984).
[41] S. Eriksen and R. G. Egdell, Surf. Sci. **180**, 263 (1987).
[42] A. G. Thomas, W. R. Flavell, C. Chatwin, D. Tsoutsou, S. Rayner, A. R. Kumarasinghe, D. Brete, T. K. Johal, S. Patel, and J. Purton, Surf. Sci. **592**, 159 (2005).
[43] O. Bikonda, C. L. Pang, R. Ithnin, C. A. Muryn, H. Onishi, and G. Thornton, Nat. Mater. **5**, 189 (2006).
[44] D. Shuttleworth, J. Phys. Chem. **84**, 1629 (1980).
[45] T. Dickinson, A. F. Povey, and P. M. A Sherwood, J. Chem. Soc., Faraday Trans. 1 **72**, 686 (1976).
[46] M. Oku, K. Hirokawa, and S. Ikada, J. Electron Spectrosc. Relat. Phenom. **7**, 465 (1975).
[47] H. W. Nesbitt, D. Legrand, and C. M. Bancroft, Phys. Chem. Miner. **27**, 357 (2000).
[48] G. van der Laan, Phys. Rev. B **41**, 12366 (1990).
[49] R. Ruus, A. Kikas, A. Saar, A. Ausmees, E. Nömmiste, J. Aarik, A. Aidla, T. Uustare, and I. Martinson, Solid State Commun. **104**, 199 (1997).
[50] J. P. Crocombette and F. Jollet, J. Phys.: Condens. Matter **6**, 10811 (1994).
[51] S. C. Lu and J. C. Falconer, J. Catal. **185**, 393 (1999).
[52] M. Anpo, M. Aikawa, Y. Kubokawa, M. Che, C. Louis, and E. Giamello, J. Phys. Chem. **89**, 5694 (1995).
[53] C. A. Jenkins and D. A. Murphy, J. Phys. Chem. B **105**, 1019 (2001).
[54] M. A. Henderson, W. S. Epling, C. L. Perkins, C. H. F. Peden, and U. Diebold, J. Phys. Chem. B **103**, 5328 (1999).
[55] T. U. Kampen, G. Gavrila, H. Mendez, D. R. T. Zahn, A. R. Vearey-Roberts, D. A. Evans, J. Wells, I. McGovern, and W. Braun, J. Phys.: Condens. Matter **15**, S2679 (2003).